Fast Method for Accelerating Time-Domain Solutions of Ill-Conditioned Electromagnetic Problems by Changing Curl–Curl Operator to Laplacian

Li Xue and Dan Jiao, *Fellow, IEEE*

***Abstract*— The ill-conditioned numerical system arising from an electromagnetic analysis is often due to the discretized curl–curl operator which has both zero eigenvalues and large ones inversely proportional to the square of the smallest feature size. In this work, we analytically decompose the discretized curl–curl operator into a gradient divergence operator and a Laplacian without numerical computation. We further split the field solution into a gradient field (curl-free component) and a divergence-free one to take advantage of the decomposition. The gradient divergence operator vanishes when acting on the divergence-free component of the field solution. As a result, we can replace the highly ill-conditioned curl–curl operator with a Laplacian for computing the divergence-free component regardless of inhomogeneity and source settings. Since the Laplacian is positive definite and well-conditioned, the new system matrix can converge quickly in a small number of iterations. The method is applied to accelerate time-domain solutions of Maxwell's equations in ill-conditioned problems such as integrated circuits (ICs). Numerical results have validated its accuracy and efficiency.**

***Index Terms*— Curl–curl operator, fast method, full-wave analysis, ill-conditioned systems, implicit time-domain method, integrated circuits (ICs), iterative solvers, large-scale analysis, layout extraction, layout modeling, layout simulation, Maxwell's equations, on-chip circuits, time-domain method.**

I. Introduction

ILL-CONDITIONED problems are frequently encountered in electromagnetic analysis. A representative class of ill-conditioned problems is the integrated circuit (IC) problem. Such a problem is large scale and deeply multiscaled. The underlying materials are inhomogeneous, and the conductors are lossy. Furthermore, broadband of frequencies from dc to high frequencies needs to be considered. In this band, both static (gradient field) and full-wave components (whose curl is not zero) co-exist in the field solution. The two also couple with each other. We cannot solve static equations alone. Meanwhile, the frequency is not that high; we cannot ignore the static component either in the field solution.

There have been a large number of efforts addressing the aforementioned challenges [1]–[18], including both frequency- and time-domain methods, spanning the partial differential equation (PDE) solvers such as the finite difference method (FDM) [19], the finite element method (FEM) [20], and the integral equation (IE)-based method. In the frequency domain, the system matrix resulting from the discretization of an ill-conditioned problem like ICs has a large condition number, and it is indefinite, which renders an iterative solution difficult to converge and a direct solution challenging to obtain an accurate solution. In the time domain, the system matrix can be made positive definite in a PDE solver. However, the time step is restricted by the smallest space step in a conventional explicit time marching for stability. In an ill-conditioned problem, the time step restricted by the stability criterion can be orders of magnitude smaller than that required by sampling accuracy for a given input spectrum. This makes a traditional explicit simulation not efficient for solving ill-conditioned problems. In an implicit unconditionally stable time domain method, the time step can be enlarged and it is independent of the space step, however, one has to solve an ill-conditioned system matrix.

In existing methods, there are two major approaches to solving an ill-conditioned numerical system. One is fast and error-controlled direct solvers such as [21]–[23]. The other is iterative solvers. The latter can preserve the sparsity of the original system matrix in a PDE-based method. Existing techniques to expedite an iterative PDE solution are mainly based on finding a good preconditioner for solving the underlying sparse system of equations [24]–[27]. Among these techniques, diagonal, block diagonal, Jacob, symmetric successive over-relaxation (SSOR) preconditioners, and so on are computationally efficient to construct. But their performance is not reliable and it is problem-dependent. Another type is to use approximate inverse or incomplete factorization-based preconditioners. This kind of preconditioners is more robust and can exhibit a faster convergence. However, they are computationally expensive. Other preconditioners suffer

Manuscript received April 23, 2021; revised July 10, 2021; accepted August 9, 2021. Date of publication September 20, 2021; date of current version November 4, 2021. This work was supported by the Defense Advanced Research Projects Agency (DARPA) under Award FA8650-18-2-7847. *(Corresponding author: Dan Jiao.)*

The authors are with the School of Electrical and Computer Engineering, Purdue University, West Lafayette, IN 47907 USA (e-mail: djiao@purdue.edu).

Color versions of one or more figures in this article are available at https://doi.org/10.1109/TMTT.2021.3108549.

Digital Object Identifier 10.1109/TMTT.2021.3108549

from a similar performance and cost tradeoff. In this work, we propose a different method to accelerate the iterative solution of an ill-conditioned full-wave system of equations. This method is to directly change the original system to its Laplacian counterpart to solve without any approximation.

We analyze the property of the system matrix resulting from a PDE-based full-wave analysis. We find that the system matrix representing the curl–curl operator is the root cause of its slow convergence. This matrix's smallest eigenvalue is zero, whereas its largest one is inversely proportional to the square of the smallest feature size in the problem being studied. In an IC problem, this translates to a huge condition number. To overcome this problem, we find a way to decompose the discretized curl–curl operator into a gradient divergence operator and a Laplacian. We also achieve such a decomposition without any numerical computation, by constructing both operators via an analytical means. To take advantage of the good property of the Laplacian, we further split the field into a gradient field (curl-free) and a divergence-free component to solve, instead of solving the unknown field as a whole. The gradient divergence operator vanishes when acting on the divergence-free component of the field. Hence, we can replace the curl–curl operator by the Laplacian when it operates on the divergence-free component of the field solution. Meanwhile, the curl–curl operator vanishes when it acts on the gradient field component. As a result, the transformed numerical system is composed of Laplacian operators only for solving both the curl-free and divergence-free components. Since the Laplacian is full-rank and well-conditioned, the updated system matrix can be converged in a very small number of iterations, whose number does not grow with the matrix size either. Meanwhile, no theoretical approximation is made, and the accuracy is retained. In [28], we presented this idea to accelerate the frequency-domain solution of full-wave Maxwell's equations. In this paper, we show how to accelerate time-domain solutions of Maxwell's equations. We develop new formulations in the time domain to fully utilize the analytical decomposition of the curl–curl operator and the good property of Laplacian, based on which we solve challenging ill-conditioned problems like ICs, where static and full-wave field solutions co-exist, and conductors are highly lossy.

It is worth mentioning that the proposed work is very different from methods in [29]–[32]. In those methods, the divergence of **D** or **J** condition is imposed to solve the two curl equations of the Maxwell's equations, whereas we only solve the two curl equations without imposing the divergence condition. Note that the divergence of **D** equation is implicitly satisfied by the curl of **H** equation, i.e., Ampere's law. In [29]–[32], the gradient of divergence (being zero) is then added in the curl–curl equation to improve the conditioning of the resultant numerical system. Since the gradient of divergence of **D** is *not* equal to zero in regions where sources exist, or in conductors, and so on, only part of the computational domain is affected by this addition. Furthermore, in an inhomoegenous problem where permittivity ϵ is nonuniform, the augmentation of the gradient of the divergence of $\epsilon\mathbf{E}$ does not turn the curl–curl of **E** into a Laplacian either. Methods in [29]–[32] have to scale the gradient divergence term with the goal of producing a term close to Laplacian in matrix norm, but the scaled term does not yield an exact Laplacian either. In contrast, we directly work on the discrete curl–curl operator to decompose it into a discrete gradient divergence and a Laplacian. This decomposition is always true regardless of nonuniform permittivity and nonzero sources. We thus obtain an exact Laplacian and also in the entire computational domain. We further split the electric field into a gradient field and a divergence-free component to solve, instead of solving the field as a whole, to take advantage of the decomposition. The proposed work can be used to effectively solve problems concerned in [29]–[32] as well.

The rest of the article is organized as follows. In Section II, we elaborate the proposed method. In Section III, we present extensive numerical results to demonstrate the accuracy and efficiency of the proposed method in solving ill-conditioned problems. We summarize this work in Section IV.

II. Proposed Method

Discretizing the entire physical layout of an IC or other physical problems into a mesh including lossy conductors and inhomogeneous dielectric materials, let **e** be a vector of all electric field unknowns in the mesh, whose length is N_e.

A PDE-based solution of full-wave Maxwell's equations results in the following linear system of equations in time domain [33], [34]:

$$\overline{\mathbf{D}}_\epsilon \frac{d^2\mathbf{e}}{dt^2} + \overline{\mathbf{D}}_\sigma \frac{d\mathbf{e}}{dt} + \overline{\mathbf{S}}\mathbf{e} = -\frac{d\mathbf{J}}{dt} \tag{1}$$

where **J** is a vector of current density, $\overline{\mathbf{D}}_\epsilon$ and $\overline{\mathbf{D}}_\sigma$ are sparse matrices associated with permittivity and conductivity, respectively. If using a finite difference time domain (FDTD), both $\overline{\mathbf{D}}_\epsilon$ and $\overline{\mathbf{D}}_\sigma$ are diagonal whose ith entry represents the permittivity and conductivity at the ith edge. If using an FEM, $\overline{\mathbf{D}}_\epsilon$ and $\overline{\mathbf{D}}_\sigma$ are related to the mass matrix, i.e., the inner product of vector basis functions used to expand unknown electric fields.

The $\overline{\mathbf{S}}$ in (1) is a sparse matrix representing a discretized $\nabla \times \mu^{-1}\nabla \times$ operation. As an example, in the FDTD, $\overline{\mathbf{S}}$ can be written as the following [33]:

$$\overline{\mathbf{S}} = \overline{\mathbf{S}}_h \overline{\mathbf{D}}_{1/\mu} \overline{\mathbf{S}}_e \tag{2}$$

where $\overline{\mathbf{S}}_h$ has N_h columns, $\overline{\mathbf{S}}_e$ has N_h rows, and N_h is the total number of patches, which is also the number of magnetic field unknowns. The $\overline{\mathbf{D}}_{1/\mu}$ is nothing but a diagonal matrix of the inverse of permeability. As another example, in the FEM, $\overline{\mathbf{S}}$ can be written as the following:

$$\overline{\mathbf{S}} = \frac{1}{\mu}\int (\nabla \times \mathbf{N}_i \cdot \nabla \times \mathbf{N}_j) dV \tag{3}$$

where **N** denotes the vector basis function used in each element to expand unknown electric fields, and the integration is performed over the computational domain V.

The $\overline{\mathbf{S}}$ is rank deficient, whose smallest eigenvalue is zero; and largest one is inversely proportional to the square of the smallest feature size. This renders the condition number of $\overline{\mathbf{S}}$ extremely large when modeling micro- and nano-meter scale structures. Inspired by the vector identity

$\nabla \times \nabla \times \mathbf{A} = \nabla(\nabla \cdot \mathbf{A}) - \nabla^2\mathbf{A}$, we find that matrix $\overline{\mathbf{S}}$ can be decomposed into the following form:

$$\overline{\mathbf{S}} = -\overline{\mathbf{V}}_0\overline{\mathbf{V}}_{0a}^T/\mu + \overline{\mathbf{L}} \tag{4}$$

where $\overline{\mathbf{V}}_0$ denotes the right nullspace of $\overline{\mathbf{S}}$, thus

$$\overline{\mathbf{S}}\overline{\mathbf{V}}_0 = 0 \tag{5}$$

and $\overline{\mathbf{V}}_{0a}^T$ denotes the left nullspace of $\overline{\mathbf{S}}$, satisfying

$$\overline{\mathbf{V}}_{0a}^T\overline{\mathbf{S}} = 0 \tag{6}$$

and $\overline{\mathbf{L}}$ denotes the discretized Laplacian $-\nabla^2$ divided by μ. To understand (4), one should realize that $\overline{\mathbf{S}}$ denotes a discretized $\nabla \times \mu^{-1}\nabla \times$ operation. Hence, its right nullspace is a gradient field (represented by $\overline{\mathbf{V}}_0$ in (4)), whereas its left nullspace is a divergence field (represented by $\overline{\mathbf{V}}_{0a}^T$). If using the FDM, in a uniform grid, $\overline{\mathbf{V}}_0 = \overline{\mathbf{V}}_{0a}$ since $\overline{\mathbf{S}}$ is symmetric. If using the FEM with a symmetric formulation, $\overline{\mathbf{V}}_0 = \overline{\mathbf{V}}_{0a}$ holds true irrespective of the regularity of the mesh.

We further find that both $\overline{\mathbf{V}}_0$ and $\overline{\mathbf{V}}_{0a}$ can be constructed from mesh information analytically. Hence the decomposition shown in (4) can be achieved without any computational cost. Specifically, the $\overline{\mathbf{V}}_0$'s column number is equal to the number of nodes -1 in the mesh. The ith column of $\overline{\mathbf{V}}_0$ corresponds to the ith node, the number of nonzero entries in which is equal to the number of edges connected to node i. At each node in the mesh, we can generate one column of $\overline{\mathbf{V}}_0$ as the following without any need for numerical computation [35].

1) For the edge whose electric field reference direction enters the node, the nonzero entry is $(1/l_i)$, at the row corresponding to the global index of the edge (and thereby its $\mathbf{E}$ unknown).
2) For the edge whose electric field reference direction leaves the node, the nonzero entry is $-(1/l_i)$,

where l_i is the length of the ith edge. The above is true for both the FDM in a grid and the FEM in an irregular mesh. The left nullspace $\overline{\mathbf{V}}_{0a}$ can also be generated without any need for computation. It is the same as $\overline{\mathbf{V}}_0$ in the FEM, or the FDM using a uniform grid. When using the FDM in a nonuniform grid, the $\overline{\mathbf{V}}_{0a}$ is different from $\overline{\mathbf{V}}_0$. But the only difference is to change the length to an *a*verage length, which is also the reason why we use subscript a to denote the left nullspace. Specifically, each node corresponds to one column of $\overline{\mathbf{V}}_{0a}$, which can be built as follows.

1) For the edge whose electric field reference direction enters the node, the nonzero entry is $(1/l_{i,\text{ave}})$, at the row corresponding to the global index of the edge (and thereby its $\mathbf{E}$ unknown).
2) For the edge whose electric field reference direction leaves the node, the nonzero entry is $-(1/l_{i,\text{ave}})$.

Where the average length $l_{i,\text{ave}}$ is the length averaged from the edge and the other edge connected to the node along the same direction. One can readily verify that (5) and (6) are satisfied in the FDM and FEM, using the $\overline{\mathbf{V}}_0$ and $\overline{\mathbf{V}}_{0a}$ analytically constructed in the aforementioned way.

Let $\overline{\mathbf{V}}_h$ be $\overline{\mathbf{S}}$'s eigenvector whose eigenvalue λ is nonzero, then $\overline{\mathbf{S}}\overline{\mathbf{V}}_h = \lambda\overline{\mathbf{V}}_h$ holds true, and hence

$$\overline{\mathbf{V}}_{0a}^T\overline{\mathbf{V}}_h = \overline{\mathbf{V}}_{0a}^T\overline{\mathbf{S}}\overline{\mathbf{V}}_h/\lambda = 0 \tag{7}$$

using (6). As a result, we find the following important property:

$$\overline{\mathbf{S}}\overline{\mathbf{V}}_h = -\overline{\mathbf{V}}_0\overline{\mathbf{V}}_{0a}^T\overline{\mathbf{V}}_h/\mu + \overline{\mathbf{L}}\overline{\mathbf{V}}_h = \overline{\mathbf{L}}\overline{\mathbf{V}}_h. \tag{8}$$

This means when operating on the high-frequency modes whose curl is not zero, we can replace $\overline{\mathbf{S}}$ by $\overline{\mathbf{L}}$! Compared to $\overline{\mathbf{S}}$, $\overline{\mathbf{L}}$ is of full rank and well-conditioned with a low condition number, as it is a Laplace operator. Many iterative solvers can solve a Laplace operator fast, and even converge it in a constant number of operations independent of matrix size [36].

If the solution of (1) is dominated by the full-wave component whose curl is nonzero, then we can directly replace $\overline{\mathbf{S}}$ therein by $\overline{\mathbf{L}}$, and solve it efficiently. But for problems involving both static and full-wave solutions, we need to carefully develop algorithms to fully take advantage of (8). Next, we show such an algorithm in the time domain.

We discretize (1) in the time domain as the following:

$$\overline{\mathbf{D}}_\epsilon(\mathbf{e}^{n+1} + \mathbf{e}^{n-1} - 2\mathbf{e}^n) + \Delta t\overline{\mathbf{D}}_\sigma(\mathbf{e}^{n+1} - \mathbf{e}^n) + \Delta t^2\overline{\mathbf{S}}\mathbf{e}^{n+1} = -\Delta t^2\frac{\partial \mathbf{J}^{n+1}}{\partial t} \tag{9}$$

where $\mathbf{e}^{n+1}$, $\mathbf{e}^n$ and $\mathbf{e}^{n-1}$ denotes the electrical field solutions at the $(n+1)$th, nth and $(n-1)$th time step, respectively, and Δt is the time step. Moving all the terms associated with previous time steps to the right-hand side, we obtain

$$\left(\overline{\mathbf{D}}_\epsilon + \Delta t\overline{\mathbf{D}}_\sigma + \Delta t^2\overline{\mathbf{S}}\right)\mathbf{e}^{n+1} = -\Delta t^2\frac{\partial \mathbf{J}^{n+1}}{\partial t} - \overline{\mathbf{D}}_\epsilon\left(\mathbf{e}^{n-1} - 2\mathbf{e}^n\right) - \Delta t\overline{\mathbf{D}}_\sigma(-\mathbf{e}^n). \tag{10}$$

The above is the so-called backward difference scheme [34], which is unconditionally stable, and hence allowing for the use of an arbitrarily large time step irrespective of space step. One can also use other unconditionally stable methods to discretize (1) in time such as the Newmark method [34], the Crank-Nicholson method, and so on. However, all of them need to solve a system matrix, and this system matrix is a weighted sum of $\mathbf{D}_\epsilon$, $\mathbf{D}_\sigma$, and $\mathbf{S}$ matrices. In what follows, we will use the system matrix resulting from the backward difference to present the proposed method, but the method is equally applicable to other implicit time marching schemes.

From (10), it can be seen that one has to solve the following system matrix:

$$\left(\overline{\mathbf{D}}_\epsilon + \Delta t\overline{\mathbf{D}}_\sigma + \Delta t^2\overline{\mathbf{S}}\right). \tag{11}$$

This matrix is ill-conditioned especially when Δt is large. This is because the ratio of $\Delta t^2\overline{\mathbf{S}}$ to $\overline{\mathbf{D}}_\epsilon$ is the ratio of $\Delta t^2/\Delta t_a^2$, where Δt_a is the time step restricted by the space step as that determined by the CFL condition. Clearly, the larger the Δt, the more important the term of $\Delta t^2\overline{\mathbf{S}}$ as compared to $\overline{\mathbf{D}}_\epsilon$ term. For a time step ten times larger than the CFL condition, the $\overline{\mathbf{D}}_\epsilon$ term already becomes negligible, as it is 100 times smaller than $\Delta t^2\overline{\mathbf{S}}$. Since $\overline{\mathbf{S}}$ is singular, numerically, its solution is difficult to converge. When there is conductor loss, $\overline{\mathbf{D}}_\sigma$ term exists and also it is orders of magnitude different from $\overline{\mathbf{D}}_\epsilon$, which makes an iterative solution of (11) even more difficult to converge.

To utilize (8), we decompose the field solution into two parts

$$\mathbf{e} = \overline{\mathbf{V}}_0\mathbf{y}_0 + \mathbf{e}_h \tag{12}$$

where $\overline{\mathbf{V}}_0\mathbf{y}_0$ is its gradient component, and $\mathbf{e}_h$ is its $\overline{\mathbf{V}}_h$ component, so that (8) can be utilized to speed up the solution of high-frequency components. The (12) can be rewritten as

$$\mathbf{e} = \begin{bmatrix}\overline{\mathbf{V}}_0 & \mathbf{I}\end{bmatrix}\begin{bmatrix}\mathbf{y}_0\\ \mathbf{e}_h\end{bmatrix} \tag{13}$$

which is equivalent to using the column space of $\begin{bmatrix}\overline{\mathbf{V}}_0 & \mathbf{I}\end{bmatrix}$ to expand the field solution. To find out the unknown coefficient vector $\begin{bmatrix}\mathbf{y}_0\\ \mathbf{e}_h\end{bmatrix}$, we can substitute (13) into (10), and also test the resultant equation by the transpose of the column space used to expand $\mathbf{e}$, thus using the following to multiply (10) in front:

$$\begin{bmatrix}\overline{\mathbf{V}}_{0a}^T\\ \mathbf{I}\end{bmatrix}. \tag{14}$$

As a result, we obtain

$$\begin{bmatrix}\overline{\mathbf{V}}_{0a}^T\\ \mathbf{I}\end{bmatrix}\left(\overline{\mathbf{D}}_\epsilon + \Delta t\overline{\mathbf{D}}_\sigma + \Delta t^2\overline{\mathbf{S}}\right)\begin{bmatrix}\overline{\mathbf{V}}_0 & \mathbf{I}\end{bmatrix}\begin{bmatrix}\mathbf{y}_0^{n+1}\\ \mathbf{e}_h^{n+1}\end{bmatrix} = \begin{bmatrix}\overline{\mathbf{V}}_{0a}^T\\ \mathbf{I}\end{bmatrix}\left(-\Delta t^2\frac{\partial \mathbf{J}^{n+1}}{\partial t} - \overline{\mathbf{D}}_\epsilon\left(\mathbf{e}^{n-1} - 2\mathbf{e}^n\right) - \Delta t\overline{\mathbf{D}}_\sigma(-\mathbf{e}^n)\right) \tag{15}$$

which can be rewritten as

$$\begin{bmatrix}\overline{\mathbf{V}}_{0a}^T\left(\overline{\mathbf{D}}_\epsilon + \Delta t\overline{\mathbf{D}}_\sigma\right)\overline{\mathbf{V}}_0 & \overline{\mathbf{V}}_{0a}^T\left(\overline{\mathbf{D}}_\epsilon + \Delta t\overline{\mathbf{D}}_\sigma\right)\\ \left(\overline{\mathbf{D}}_\epsilon + \Delta t\overline{\mathbf{D}}_\sigma\right)\overline{\mathbf{V}}_0 & \overline{\mathbf{D}}_\epsilon + \Delta t\overline{\mathbf{D}}_\sigma + \Delta t^2\overline{\mathbf{S}}\end{bmatrix}\begin{bmatrix}\mathbf{y}_0^{n+1}\\ \mathbf{e}_h^{n+1}\end{bmatrix} = \begin{bmatrix}\overline{\mathbf{V}}_{0a}^T\mathbf{b}\\ \mathbf{b}\end{bmatrix} \tag{16}$$

where

$$\mathbf{b} = -\Delta t^2\frac{\partial \mathbf{J}^{n+1}}{\partial t} - \overline{\mathbf{D}}_\epsilon\left(\mathbf{e}^{n-1} - 2\mathbf{e}^n\right) - \Delta t\overline{\mathbf{D}}_\sigma(-\mathbf{e}^n). \tag{17}$$

In the first row of (16), $\overline{\mathbf{S}}$ vanishes because of (6); whereas in the second row of equation, $\overline{\mathbf{S}}$ vanishes in the first term because of (5).

The only $\overline{\mathbf{S}}$ left in (16) operates on $\mathbf{e}_h^{n+1}$, which is in the space of $\overline{\mathbf{V}}_h$. Using (8), we can replace $\overline{\mathbf{S}}$ by $\overline{\mathbf{L}}$, obtaining

$$\begin{bmatrix}\overline{\mathbf{V}}_{0a}^T\left(\overline{\mathbf{D}}_\epsilon + \Delta t\overline{\mathbf{D}}_\sigma\right)\overline{\mathbf{V}}_0 & \overline{\mathbf{V}}_{0a}^T\left(\overline{\mathbf{D}}_\epsilon + \Delta t\overline{\mathbf{D}}_\sigma\right)\\ \left(\overline{\mathbf{D}}_\epsilon + \Delta t\overline{\mathbf{D}}_\sigma\right)\overline{\mathbf{V}}_0 & \overline{\mathbf{D}}_\epsilon + \Delta t\overline{\mathbf{D}}_\sigma + \Delta t^2\overline{\mathbf{L}}\end{bmatrix}\begin{bmatrix}\mathbf{y}_0^{n+1}\\ \mathbf{e}_h^{n+1}\end{bmatrix} = \begin{bmatrix}\overline{\mathbf{V}}_{0a}^T\mathbf{b}\\ \mathbf{b}\end{bmatrix}. \tag{18}$$

As a result, the lower right block of the system matrix becomes a well-conditioned matrix to solve. Notice that $\overline{\mathbf{L}}$ is positive-definite and of full rank.

If we solve (18) as it is, although the entire system matrix is composed of well-conditioned submatrices, the convergence of its iterative solution can be slow because the submatrices are very different in magnitude, and hence unbalanced. We, therefore, propose to use the following $\overline{\mathbf{P}}$ as a preconditioner to solve (18), thus

$$\overline{\mathbf{P}} = \begin{bmatrix}\overline{\mathbf{V}}_{0a}^T\left(\overline{\mathbf{D}}_\epsilon + \Delta t\overline{\mathbf{D}}_\sigma\right)\overline{\mathbf{V}}_0 & \overline{\mathbf{V}}_{0a}^T\left(\overline{\mathbf{D}}_\epsilon + \Delta t\overline{\mathbf{D}}_\sigma\right)\\ & \overline{\mathbf{D}}_\epsilon + \Delta t\overline{\mathbf{D}}_\sigma + \Delta t^2\overline{\mathbf{L}}\end{bmatrix}. \tag{19}$$

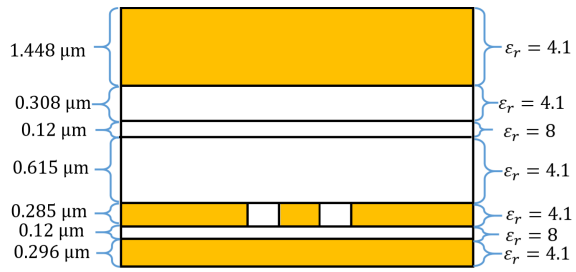

Fig. 1. Structure of a test-chip interconnect.

Using the above, the solution of (18) is found to converge in a very small number of iterations. This is because the off-diagonal block is much smaller than the diagonal one in the second block row of (18) in an ill-conditioned problem.

In (19), in order to solve $\overline{\mathbf{V}}_{0a}^T(\overline{\mathbf{D}}_\epsilon + \Delta t\overline{\mathbf{D}}_\sigma)\overline{\mathbf{V}}_0$ fast, we further transform it to the solution of two Laplacians as follows. We expand the static component $\overline{\mathbf{V}}_0\mathbf{y}_0$ into

$$\overline{\mathbf{V}}_0\mathbf{y}_0 = \overline{\mathbf{V}}_{0d}\mathbf{y}_{0d} + \overline{\mathbf{V}}_{0c}\mathbf{y}_{0c} \tag{20}$$

where $\overline{\mathbf{V}}_{0d}$ are the $\overline{\mathbf{V}}_0$ columns associated with the dielectric nodes, and $\overline{\mathbf{V}}_{0c}$ are those associated with conductor nodes. Then the $\overline{\mathbf{V}}_{0a}^T(\overline{\mathbf{D}}_\epsilon + \Delta t\overline{\mathbf{D}}_\sigma)\overline{\mathbf{V}}_0$ subsystem of equations can be rewritten as

$$\begin{bmatrix}\overline{\mathbf{V}}_{0da}^T(\overline{\mathbf{D}}_\epsilon)\overline{\mathbf{V}}_{0d} & \overline{\mathbf{V}}_{0da}^T(\overline{\mathbf{D}}_\epsilon)\overline{\mathbf{V}}_{0c}\\ \overline{\mathbf{V}}_{0ca}^T(\overline{\mathbf{D}}_\epsilon)\overline{\mathbf{V}}_{0d} & \overline{\mathbf{V}}_{0ca}^T(\overline{\mathbf{D}}_\epsilon + \Delta t\overline{\mathbf{D}}_\sigma)\overline{\mathbf{V}}_{0c}\end{bmatrix}\begin{bmatrix}\mathbf{y}_{0d}\\ \mathbf{y}_{0c}\end{bmatrix} = \begin{bmatrix}\mathbf{b}_{0d}\\ \mathbf{b}_{0c}\end{bmatrix} \tag{21}$$

where $\overline{\mathbf{V}}_{0d}$, $\overline{\mathbf{V}}_{0da}$, $\overline{\mathbf{V}}_{0c}$, $\overline{\mathbf{V}}_{0ca}$ are all normalized, $\overline{\mathbf{V}}_{0da}$ and $\overline{\mathbf{V}}_{0ca}$ are left nullspace vectors, and $\mathbf{b}_{0d}$ and $\mathbf{b}_{0c}$ are corresponding right-hand sides. The above can be written in short as

$$\begin{bmatrix}\overline{\mathbf{M}}_{\mathrm{dd}} & \overline{\mathbf{M}}_{\mathrm{dc}}\\ \overline{\mathbf{M}}_{\mathrm{cd}} & \overline{\mathbf{M}}_{\mathrm{cc}}\end{bmatrix}\begin{bmatrix}\mathbf{y}_{0d}\\ \mathbf{y}_{0c}\end{bmatrix} = \begin{bmatrix}\mathbf{b}_{0d}\\ \mathbf{b}_{0c}\end{bmatrix} \tag{22}$$

where

$$\overline{\mathbf{M}}_{\mathrm{dd}} = \overline{\mathbf{V}}_{0da}^T(\overline{\mathbf{D}}_\epsilon)\overline{\mathbf{V}}_{0d} \tag{23}$$

$$\overline{\mathbf{M}}_{\mathrm{dc}} = \overline{\mathbf{V}}_{0da}^T(\overline{\mathbf{D}}_\epsilon)\overline{\mathbf{V}}_{0c} \tag{24}$$

$$\overline{\mathbf{M}}_{\mathrm{cd}} = \overline{\mathbf{V}}_{0ca}^T(\overline{\mathbf{D}}_\epsilon)\overline{\mathbf{V}}_{0d} \tag{25}$$

$$\overline{\mathbf{M}}_{\mathrm{cc}} = \overline{\mathbf{V}}_{0ca}^T(\overline{\mathbf{D}}_\epsilon + \Delta t\overline{\mathbf{D}}_\sigma)\overline{\mathbf{V}}_{0c}. \tag{26}$$

Note that $\overline{\mathbf{M}}_{\mathrm{cc}}$ is inside conductors, and hence the displacement current is much smaller than the conduction current. Then the term $(\overline{\mathbf{D}}_\epsilon)$ can be ignored. Therefore, we have

$$\overline{\mathbf{M}}_{\mathrm{cc}} \approx \overline{\mathbf{V}}_{0ca}^T(\Delta t\overline{\mathbf{D}}_\sigma)\overline{\mathbf{V}}_{0c}. \tag{27}$$

To solve (22), first, we solve the Schur complement of the $\overline{\mathbf{M}}_{\mathrm{dd}}$, which is

$$\left(\overline{\mathbf{M}}_{\mathrm{dd}} - \overline{\mathbf{M}}_{\mathrm{dc}}\overline{\mathbf{M}}_{\mathrm{cc}}^{-1}\overline{\mathbf{M}}_{\mathrm{cd}}\right)\mathbf{y}_{0d} = \mathbf{b}_{0d} - \overline{\mathbf{M}}_{\mathrm{dc}}\overline{\mathbf{M}}_{\mathrm{cc}}^{-1}\mathbf{b}_{0c}. \tag{28}$$

Because in this matrix, $\mathbf{D}_\sigma$ dominates in magnitude and the other matrix blocks' magnitude is much smaller, we have

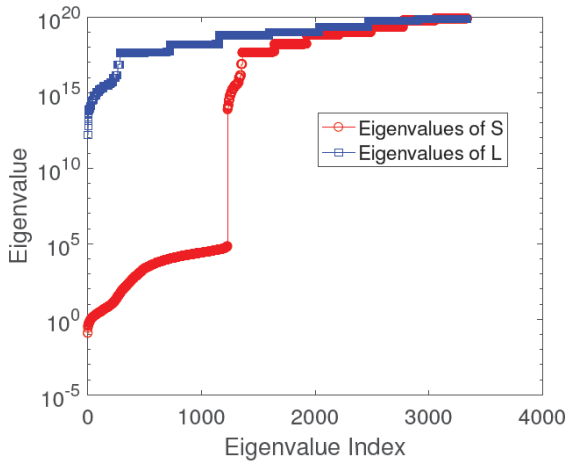

Fig. 2. Eigenvalues of $\overline{\mathbf{L}}$ as compared to those of $\overline{\mathbf{S}}$.

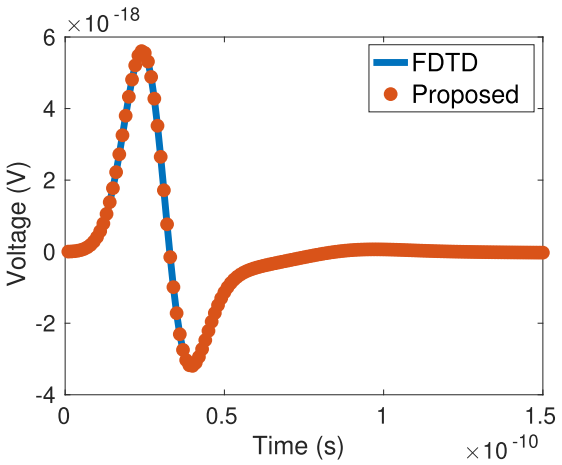

Fig. 3. Comparison between the proposed method and the traditional FDTD in simulating an on-chip interconnect.

$\|\overline{\mathbf{M}}_{\rm dd}\| \gg \|\overline{\mathbf{M}}_{\rm dc}\overline{\mathbf{M}}_{\rm cc}^{-1}\overline{\mathbf{M}}_{\rm cd}\|$. Therefore, (28) can be rewritten accurately as

$$\overline{\mathbf{M}}_{\rm dd}\mathbf{y}_{0d} = \mathbf{b}_{0d} - \overline{\mathbf{M}}_{\rm dc}\overline{\mathbf{M}}_{\rm cc}^{-1}\mathbf{b}_{0c}. \tag{29}$$

After $\mathbf{y}_{0d}$ is obtained, substitute it into the first equation, and $\mathbf{y}_{0c}$ can be computed as

$$\overline{\mathbf{M}}_{\rm cc}\mathbf{y}_{0c} = \mathbf{b}_{0c} - \overline{\mathbf{M}}_{\rm cd}\mathbf{y}_{0d}. \tag{30}$$

Note that the two diagonal blocks, denoted by $\overline{\mathbf{M}}_{\rm dd}$ and $\overline{\mathbf{M}}_{\rm cc}$, are nothing but discretized $\nabla \cdot \epsilon\nabla$ and $\nabla \cdot \sigma\nabla$ in the mesh. Hence, (29) and (30) can be rapidly solved by fast Laplacian solvers such as a multigrid iterative method, which can converge in a constant number of steps for Laplace operators.

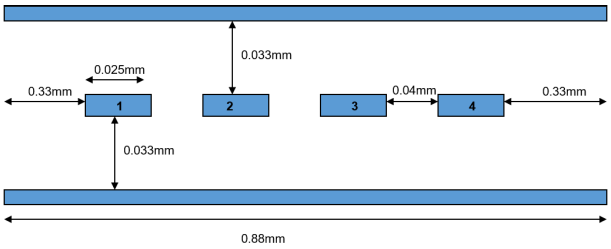

Fig. 4. Structure of an IBM plasma package interconnect.

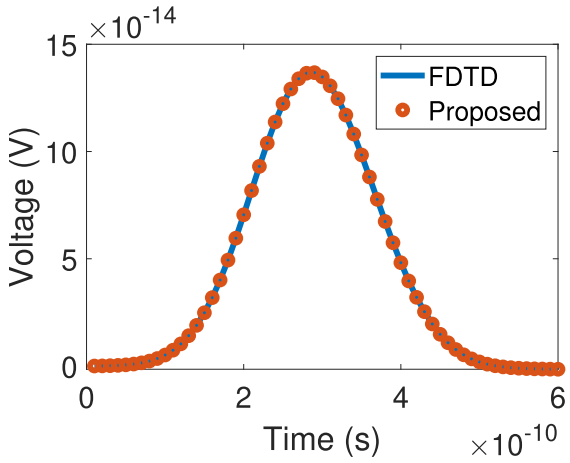

Fig. 5. Comparison between the proposed method and the traditional FDTD in simulating a package interconnect.

The preconditioner shown in (19) can further be simplified to the following upper triangular matrix:

$$\overline{\mathbf{P}} = \begin{bmatrix} \overline{\mathbf{V}}_{0\rm da}^T(\overline{\mathbf{D}}_\epsilon)\overline{\mathbf{V}}_{0d} & \overline{\mathbf{V}}_{0\rm da}^T(\overline{\mathbf{D}}_\epsilon)\overline{\mathbf{V}}_{0c} & \overline{\mathbf{V}}_{0\rm da}^T(\overline{\mathbf{D}}_\epsilon) \\ & \overline{\mathbf{V}}_{0\rm ca}^T(\Delta t\overline{\mathbf{D}}_\sigma)\overline{\mathbf{V}}_{0c} & \overline{\mathbf{V}}_{0\rm ca}^T(\overline{\mathbf{D}}_\epsilon + \Delta t\overline{\mathbf{D}}_\sigma) \\ & & \overline{\mathbf{D}}_\epsilon + \Delta t\overline{\mathbf{D}}_\sigma + \Delta t^2\overline{\mathbf{L}} \end{bmatrix}. \tag{31}$$

It can be used to effectively solve (18) because the blocks omitted are orders of magnitude smaller than the matrix blocks residing in the same block row of equations in an IC layout. Furthermore, the solution of the above preconditioner can be computed efficiently since via a backward substitution procedure, it only requires solving the three diagonal blocks, and each of which is a Laplacian, and hence can be solved fast.

III. Simulation Results

In this section, we simulate ill-conditioned on-chip, package, and antenna problems to validate the accuracy and efficiency of the proposed algorithm. We use an implicit FDTD to generate a numerical system for solving full-wave Maxwell's equations in the time domain, the solution of which is accelerated by the proposed fast method. Instead of solving (11) which is ill-conditioned, the transformed Laplacian system (18) is solved. Due to the good property of the Laplacian matrix, the iterative solution of (18) converges in a

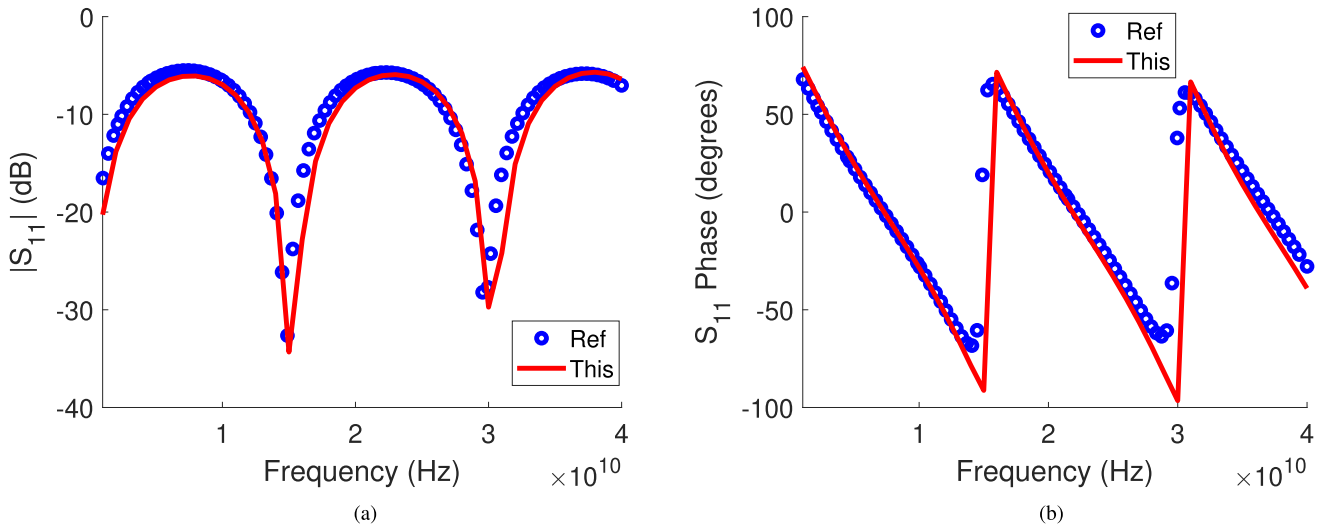

(a) (b)

Fig. 6. Comparison of the **S**-parameters between the results from the proposed method and the experimental data. (a) Magnitude. (b) Phase.

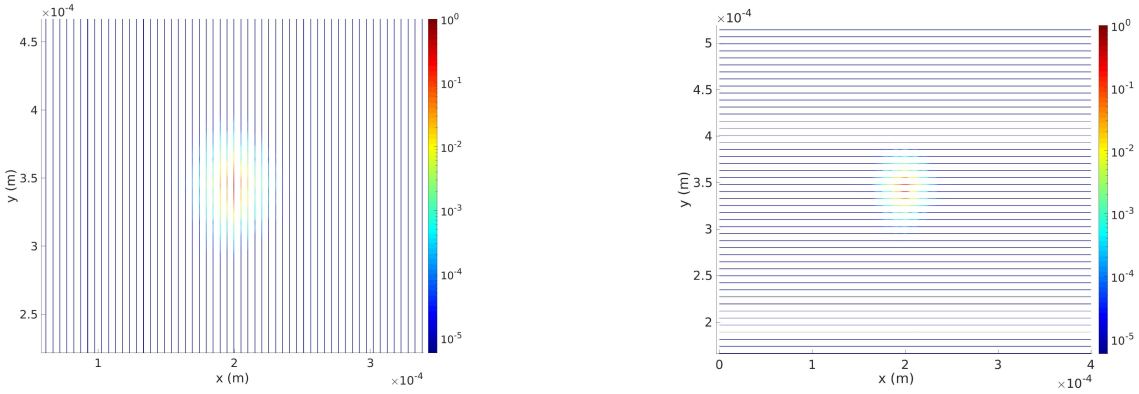

(a) (b)

Fig. 7. Voltage distribution of an on-chip power grid at 10 GHz. Power rails in (a) M5 and (b) M6 layers.

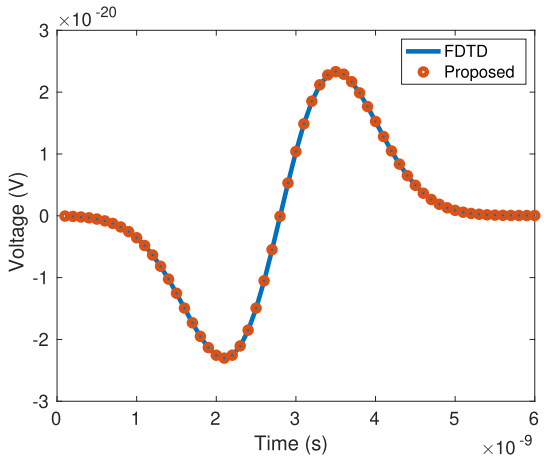

Fig. 8. Comparison between the proposed method and the traditional FDTD in simulating an on-chip power grid.

few steps to obtain the desired accuracy. The proposed method is equally applicable to the FEM and other PDE methods.

A. Test-Chip Interconnect

A test-chip interconnect is simulated, whose $x-z$ cross-sectional view is shown in Fig. 1, and it extends into the paper (y-direction) for 2000 μm. The dimensions along the x-, and z-direction are 300 μm, and 3.19 μm respectively. The yellow regions are conductors, the conductivity of which is 5.8×10^7 S/m. A nonuniform grid is used to discretize the structure, which has 23, 20, and 7 cells along x-, y-, and z-direction, respectively. The boundary conditions on all of the outermost boundaries are a Neumann boundary condition (i.e., left open), except for the bottom plane which is a perfect electric conductor (PEC). The bottom plane is used as a ground for the circuit simulation in this example.

We calculated $(\|\overline{\mathbf{S}}\overline{\mathbf{V}}_h - (\overline{\mathbf{L}}\overline{\mathbf{V}}_h)\|/(\|\overline{\mathbf{S}}\overline{\mathbf{V}}_h\|)$ and found it to be 3.3239×10^{-10}, which verifies (8). Another check we did is to evaluate $(\|\overline{\mathbf{S}} - (-\overline{\mathbf{V}}_0\overline{\mathbf{V}}_{0a}^T/\mu + \overline{\mathbf{L}})\|)/(\|\overline{\mathbf{S}}\|)$, which is found to be 3.2806×10^{-16}, and hence validating (4). In Fig. 2, we plot the eigenvalues of $\overline{\mathbf{S}}$, and $\overline{\mathbf{L}}$ respectively. It is obvious that $\overline{\mathbf{S}}$ is ill-conditioned while $\overline{\mathbf{L}}$ is not. All those eigenvalues whose magnitude is 10^5 or smaller are actually zero eigenvalues of $\overline{\mathbf{S}}$. They cannot be computed as exact zeros because of machine precision: their values are about 15 or 16 orders of magnitude smaller than the largest one. The condition number of $\overline{\mathbf{S}}$ is found to be 4.6737×10^{27}, whereas that of $\overline{\mathbf{L}}$ is only 2.5×10^8.

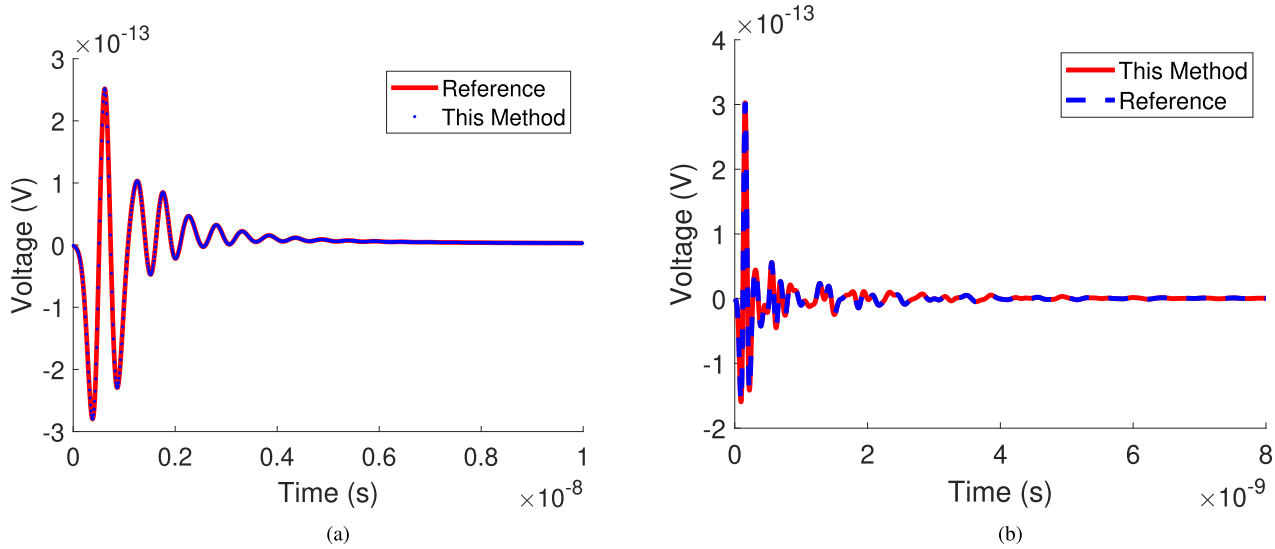

Fig. 9. Time-domain voltage of a cavity-backed patch antenna. (a) $\tau = 0.2$ ns. (b) $\tau = 0.05$ ns.

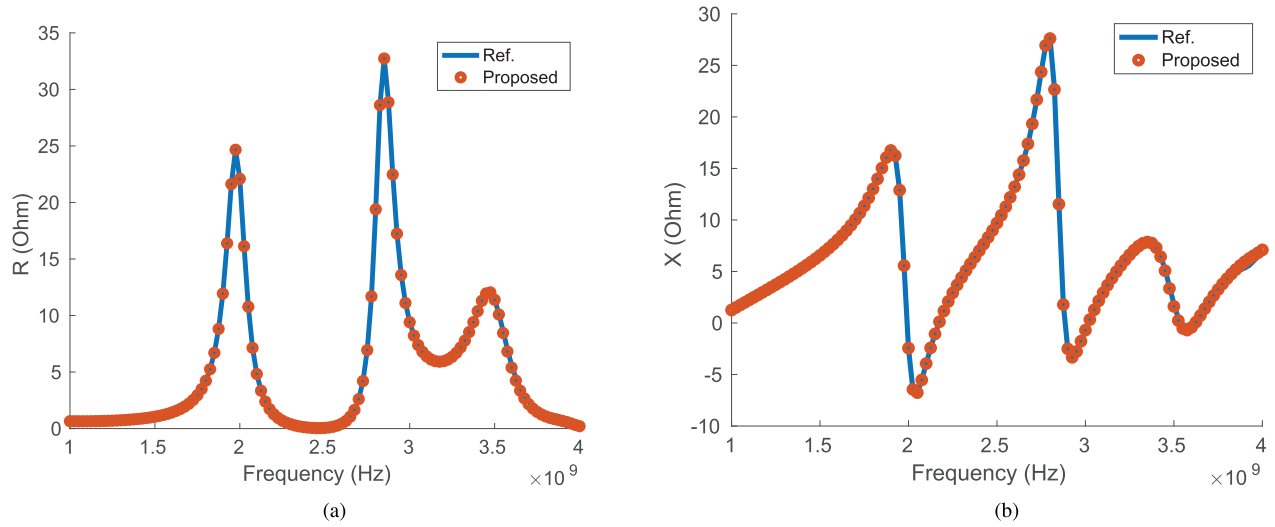

Fig. 10. Input impedance of the cavity-backed patch antenna. (a) and (b) Input resistance (Ohms).

We use a Gaussian derivative as the current source with $\tau = 10^{-11}$ s, which is injected from the bottom PEC plane to the middle conductor. The time step is chosen as $\Delta t = 10^{-12}$ s, which is solely determined by accuracy, while a conventional explicit marching must use a time step as small as 10^{-16} s in this example to ensure stability. We iteratively solve the transformed Laplacian system (18) using GMRES with (31) as the preconditioner. The GMRES solution quickly converges in 14 steps with a relative residual smaller than 10^{-5}. In contrast, if we solve the original numerical system (11), it takes 400 steps to converge, while $(\overline{\mathbf{D}}_\epsilon + \Delta t\overline{\mathbf{D}}_\sigma + \Delta t^2\overline{\mathbf{L}})$ only takes one step to reach a relative residual of 10^{-15}. When solving (22), it only takes three steps to achieve a relative residual of 10^{-5} to solve $\overline{\mathbf{M}}_{\rm dd}$. And solving $\overline{\mathbf{M}}_{\rm cc}$ takes nine steps to achieve a relative residual of 10^{-5}. The time domain voltage obtained using the proposed method is compared with that from a traditional FDTD in Fig. 3, which reveals an excellent agreement. The traditional FDTD code is what is used to simulate the same example in [18], which generates the same results as measured data as can be seen from [18, Figs. 5 and 7].

B. IBM Plasma Interconnect

The second example is an IBM plasma package interconnect, whose $x - z$ cross section is shown in Fig. 4, and it extends into the paper for 1 cm. The blue regions are conductors, with a conductivity of 5.8×10^7 S/m. The dimension along x-, y-, and z-direction is 0.88, 10, and 0.165 mm, respectively. Neumann boundary conditions are used to truncate the outermost boundaries except for the bottom plane which is a PEC. The current source is injected from the bottom plane to conductor 1 at the near end. A nonuniform Cartesian grid is used to discretize the structure, which has 22, 22, and 5 cells along the x-, y-, and z-directions, respectively. First, we calculate $(\|\overline{\mathbf{SV}}_h - \overline{\mathbf{LV}}_h\|)/(\|\overline{\mathbf{SV}}_h\|)$ and

find it to be 1.6572×10^{-12}, which again verifies (8). The $(\|\overline{\mathbf{S}} - (-\overline{\mathbf{V}}_0\overline{\mathbf{V}}_{0a}^T/\mu + \overline{\mathbf{L}})\|)/(\|\overline{\mathbf{S}}\|)$ is also evaluated, and found to be 2.8933×10^{-16}.

When solving the problem in time domain, we use GMRES with (31) as the preconditioner to ietratively solve the transformed Laplacian system. The solution is shown to converge in 14 steps, achieving a relative residual of 10^{-7}. In the preconditioner, we solve $(\overline{\mathbf{D}}_\epsilon + \Delta t\overline{\mathbf{D}}_\sigma + \Delta t^2\overline{\mathbf{L}})$ instead of $(\overline{\mathbf{D}}_\epsilon + \Delta t\overline{\mathbf{D}}_\sigma + \Delta t^2\overline{\mathbf{S}})$. The multigrid method solves $(\overline{\mathbf{D}}_\epsilon + \Delta t\overline{\mathbf{D}}_\sigma + \Delta t^2\overline{\mathbf{L}})$ with only 1 step achieving accuracy of 10^{-11}. In contrast, if $(\overline{\mathbf{D}}_\epsilon + \Delta t\overline{\mathbf{D}}_\sigma + \Delta t^2\overline{\mathbf{S}})$ is solved, it takes 500 steps to achieve an accuracy of 0.001. When solving (22), $\overline{\mathbf{M}}_{\rm dd}$ only takes tree steps to reach 10^{-5} accuracy and $\overline{\mathbf{M}}_{\rm cc}$ takes no greater than 17 steps to reach 10^{-5}. A Gaussian derivative pulse with $\tau = 10^{-10}$ s is used here as the current source. Based on the sampling accuracy, $\Delta t = 10^{-11}$ s is chosen as the time step, which is independent of the space step. The time domain voltage between conductor 1 and the ground plane simulated from the proposed method is compared with the result from a traditional FDTD in Fig. 5. Excellent agreement is observed. This example also has reference S-parameter data provided by IBM for comparison. We hence do a Fourier transform on both voltage and current source in time domain, and compare extracted frequency-domain S-parameters with IBM's reference data. As can be seen from Fig. 6, good agreement is observed.

C. On-Chip Power Grid

The third example is a large-scale on-chip power grid. It consists of four metal layers and three dielectric layers, truncated by a Neumann boundary condition, where all the boundaries are left open from the outside. The dimension along the x-, y-, and z-directions is 400, 700, and 2.838 μm, respectively. The power and ground rails are interleaved, and vias are located at the intersection of like rails in adjacent metal layers. On each metal layer, the metals are distributed periodically, the period of which is 5.12, 7.56, 10.24, and 11.34 μm, on M5, M6, M7, and M8 layers, respectively. With a nonuniform Cartesian grid, the discretization of the structure results in 4 397 222 unknowns. A current source is injected from a ground rail at ($x = 195.578$ μm, $y = 348.3$ μm) to a power one at ($x = 199.680$ μm, $y = 348.3$ μm) in the middle of the grid at the bottom metal layer, which is a Gaussian derivative pulse with $\tau = 10^{-9}$ s. The proposed method uses a large time step of $\Delta t = 10^{-10}$ s to perform time marching, which is solely determined from the input spectrum instead of space step. The voltage distributions at 10 GHz across the power grid on metal 5 and metal 6 layers are shown in Fig. 7. The voltage sampled at the input terminal is plotted in Fig. 8, and compared with the FDTD result. Good agreement is observed. This problem is solved using an upper triangular preconditioner shown in (31). It only takes six steps to reach a relative residual of 0.007. In the preconditioner, solving $(\overline{\mathbf{D}_\epsilon} + \Delta t\overline{\sigma} + \Delta t^2\overline{\mathbf{L}})$ takes three steps to achieve an accuracy of 10^{-5}. And solving $\overline{\mathbf{M}}_{\rm dd}$ takes one step to reach 10^{-5} accuracy, while for $\overline{\mathbf{M}}_{\rm cc}$, it takes no greater than 15 steps to achieve the same accuracy. In contrast, solving the original $\mathbf{S}$-based implicit time-domain system of equations takes about 300 steps to converge to a relative residual of 0.007, and costing 56 820 s in total, whereas the proposed method only takes 8989.2 s, which is more efficient.

D. Cavity-Backed Microstrip Patch Antenna

The fourth example is a cavity-backed path antenna example shown in [20]. The problem is multiscaled with the thickness of the substrate, 0.08779 cm, much smaller than other dimensions. The cavity is of size 7.5 by 5.1 cm. The antenna patch size is $W = 3.4$ cm by $L = 5$ cm. There is a 50 Ω load at the point $x_L = -2.2$ cm and $y_L = -1.5$ cm. The current is injected at the $x_f = 1.22$ cm and $y_f = 0.85$ cm point, which is a Gaussian derivative pulse with $\tau = 0.2$ ns. A nonuniform Cartesian gird is used to discretize the structure. There are 40, 38, and 3 cells along the x-, y-, and z-directions, respectively. The antenna patch is modeled with a finite conductivity of 5.8×10^7 S/m. In the time marching, a time step of $\Delta t = 10^{-11}$ s is used. The voltage obtained at the current source location is plotted in Fig. 9(a) in comparison with the reference FDTD simulation. Good agreement is observed. This problem is less ill-conditioned compared to the previous IC problems. However, the number of iterations used, 26, is still much smaller than the 158 iterations one has to use if solving the original numerical system. This example has frequency-domain reference results available in [20] from 1 to 4 GHz. We hence shortened the τ correspondingly to 0.05 ns to cover the desired frequency band, and extracted frequency-domain input impedance. The time-domain comparison with conventional FDTD is shown in Fig. 9(b), whereas the frequency-domain comparison with reference data given in [20] is shown in Fig. 10. As can be seen, good agreement is observed, which further verifies the accuracy of the proposed method.

IV. Conclusion

In this work, a fast method is developed to accelerate the time-domain solution of ill-conditioned electromagnetic problems. In this method, we perform a computation-free decomposition of the discretized curl–curl operator into a gradient divergence operator and a Laplacian. We further expand the unknown field solution into a gradient field and a divergence-free component. The former is in the nullspace of the curl–curl operator, and hence the curl–curl operator vanishes when operating on it. For the latter component (divergence-free one), the curl–curl operator can be rigorously replaced by a Laplacian. As a result, the original ill-conditioned numerical system is changed to a Laplacian-based one that is much better conditioned. Since the Laplace operator is positive definite and has guaranteed convergence in its iterative solution, we are able to significantly accelerate the time-domain solution of ill-conditioned electromagnetic problems. Numerical experiments have demonstrated its accuracy and efficiency. The method can be used to accelerate various PDE methods in time domain. In addition, not only full-wave problems, eddy-current, and magneto-quasi-static problems involving the singular curl–curl operator can also be solved by using the proposed method.

REFERENCES

[1] A. E. Ruehli, "Equivalent circuit models for three-dimensional multiconductor systems," *IEEE Trans. Microw. Theory Techn.*, vol. MTT-22, no. 3, pp. 216–221, Mar. 1974.

[2] S. Kapur and D. Long, "IES^3: A fast integral equation solver for efficient 3-dimensional extraction," *Proc. IEEE Int. Conf. Comput. Aided Design (ICCAD)*, Nov. 1997, pp. 448–455.

[3] S. Chang, R. Coccioli, Y. Qian, and T. Itoh, "A global finite-element time-domain analysis of active nonlinear microwave circuits," *IEEE Trans. Microw. Theory Techn.*, vol. 47, no. 12, pp. 2401–2416, Dec. 1999.

[4] C. C.-P. Chen, T.-W. Lee, N. Murugesan, and S. C. Hagness, "Generalized FDTD-ADI: An unconditionally stable full-wave Maxwell's equations solver for VLSI interconnect modeling," in *Proc. IEEE/ACM Int. Conf. Comput. Aided Design (ICCAD)*, Nov. 2000, pp. 156–163.

[5] J.-S. Zhao and W. C. Chew, "Integral equation solution of Maxwell's equations from zero frequency to microwave frequencies," *IEEE Trans. Antennas Propag.*, vol. 48, no. 10, pp. 1635–1645, Oct. 2000.

[6] S. Kapur and D. E. Long, "Large-scale full-wave simulation," in *Proc. 41st Annu. Conf. Design Autom. (DAC)*, 2004, pp. 806–809.

[7] Z. Zhu, B. Song, and J. White, "Algorithms in FastImp: A fast and wide-band impedance extraction program for complicated 3-D geometries," in *Proc. Design Autom. Conf.*, 2003, pp. 712–717.

[8] J.-Y. Ihm and A. C. Cangellaris, "Distributed on-chip power grid modeling: An electromagnetic alternative to RLC extraction-based models," in *Proc. Electr. Perform. Electr. Packag. (EPEP)*, 2003, pp. 37–40.

[9] A. Rong, A. C. Cangellaris, and L. Dong, "Comprehensive broadband electromagnetic modeling of on-chip interconnects with a surface discretization-based generalized PEEC model," in *Proc. Electr. Perform. Electr. Packag. (EPEP)*, Oct. 2003, pp. 367–370.

[10] D. Jiao *et al.*, "A novel technique for full-wave modeling of large-scale three-dimensional high-speed on/off-chip interconnect structures," in *Proc. Int. Conf. Simulation Semiconductor Processes Devices (SISPAD)*, 2003, pp. 39–42.

[11] Z. Cendes and A. Yen, "Mixed electromagnetic and electrical circuit simulation for RFIC characterization," in *Proc. IEEE Antennas Propag. Soc. Symp.*, Jun. 2004, pp. 3289–3292.

[12] A. E. Yilmaz, J.-M. Jin, and E. Michielssen, "A parallel FFT accelerated transient field-circuit simulator," *IEEE Trans. Microw. Theory Techn.*, vol. 53, no. 9, pp. 2851–2865, Sep. 2005.

[13] C. Yang and V. Jandhyala, "A time-domain surface integral technique for mixed electromagnetic and circuit simulation," *IEEE Trans. Adv. Packag.*, vol. 28, no. 4, pp. 745–753, Nov. 2005.

[14] Z. G. Qian *et al.*, "Crosstalk analysis by fast computational algorithms," in *Proc. IEEE 14th Topical Meeting Electr. Perform. Electron. Packag.*, Oct. 2005, pp. 367–370.

[15] H. Gan and D. Jiao, "A time-domain layered finite element reduction recovery (LAFE-RR) method for high-frequency VLSI design," *IEEE Trans. Antennas Propag.*, vol. 55, no. 12, pp. 3620–3629, Dec. 2007.

[16] R. Wang and J.-M. Jin, "A symmetric electromagnetic-circuit simulator based on the extended time-domain finite element method," *IEEE Trans. Microw. Theory Techn.*, vol. 56, no. 12, pp. 2875–2884, Dec. 2008.

[17] Q. He, D. Chen, and D. Jiao, "From layout directly to simulation: A first-principle-guided circuit simulator of linear complexity and its efficient parallelization," *IEEE Trans. Compon., Package., Manuf. Technol.*, vol. 2, no. 4, pp. 687–699, Apr. 2012.

[18] L. Xue and D. Jiao, "Rapid modeling and simulation of integrated circuit layout in both frequency and time domains from the perspective of inverse," *IEEE Trans. Microw. Theory Techn.*, vol. 68, no. 4, pp. 1270–1283, Apr. 2020.

[19] A. Taflove and S. Hagness, *Computational Electrodynamics*. Norwood, MA, USA: Artech House, 2000.

[20] J. Jin, *The Finite Element Method in Electromagn*. Hoboken, NJ, USA: Wiley, 2014.

[21] W. Chai, D. Jiao, and C.-K. Koh, "A direct integral-equation solver of linear complexity for large-scale 3D capacitance and impedance extraction," in *Proc. 46th Annu. Design Autom. Conf. (ZZZ DAC)*, 2009, pp. 752–757.

[22] W. Chai and D. Jiao, "Dense matrix inversion of linear complexity for integral-equation-based large-scale 3-D capacitance extraction," *IEEE Trans. Microw. Theory Techn.*, vol. 59, no. 10, pp. 2404–2421, Oct. 2011.

[23] B. Zhou and D. Jiao, "Direct finite-element solver of linear complexity for large-scale 3-D electromagnetic analysis and circuit extraction," *IEEE Trans. Microw. Theory Techn.*, vol. 63, no. 10, pp. 3066–3080, Oct. 2015.

[24] J. Liu and J.-M. Jin, "A highly effective preconditioner for solving the finite element-boundary integral matrix equation of 3-D scattering," *IEEE Trans. Antennas Propag.*, vol. 50, no. 9, pp. 1212–1221, Sep. 2002.

[25] Y. Yang, Z. H. Fan, D. Z. Ding, and S. B. Liu, "Application of the preconditioned GMRES to the Crank-Nicolson finite-difference time-domain algorithm for 3D full-wave analysis of planar circuits," *Microw. Opt. Technol. Lett.*, vol. 50, no. 6, pp. 1458–1463, 2008.

[26] R.-S. Chen, E. K.-N. Yung, C. H. Chan, D. X. Wang, and D. G. Fang, "Application of the SSOR preconditioned CG algorithm to the vector FEM for 3D full-wave analysis of electromagnetic-field boundary-value problems," *IEEE Trans. Microw. Theory Techn.*, vol. 50, no. 4, pp. 1165–1172, Apr. 2002.

[27] F. Sheng, H. Gan, and D. Jiao, "Fast iterative solution algorithms in the frequency-domain layered finite element method for analyzing integrated circuits," *IEEE Trans. Adv. Packag.*, vol. 33, no. 2, pp. 524–533, May 2010.

[28] L. Xue and D. Jiao, "Fast method for accelerating convergence in iterative solution of frequency-domain partial differential equation methods," in *Proc. IEEE Int. Symp. Antennas Propag. North Amer. Radio Sci. Meeting*, Jul. 2020, pp. 1003–1004.

[29] P. Hahne and T. Weiland, "3D eddy current computation in the frequency domain regarding the displacement current," *IEEE Trans. Magn.*, vol. 28, no. 2, pp. 1801–1804, Mar. 1992.

[30] M. Clemens and T. Weiland, "Regularization of eddy-current formulations using discrete grad-div operators," *IEEE Trans. Magn.*, vol. 38, no. 2, pp. 569–572, Mar. 2002.

[31] H. Dong and G. D. Egbert, "Divergence-free solutions to electromagnetic forward and adjoint problems: A regularization approach," *Geophys. J. Int.*, vol. 216, no. 2, pp. 906–918, Feb. 2019.

[32] J. Li, R. Liu, R. Guo, Y. Wang, and X. Wang, "3D finite difference modeling of controlled-source electromagnetic response in frequency domain based on a modified curl-curl equation," *J. Appl. Geophys.*, vol. 183, Dec. 2020, Art. no. 104202.

[33] J. Yan and D. Jiao, "Fast explicit and unconditionally stable FDTD method for electromagnetic analysis," *IEEE Trans. Microw. Theory Techn.*, vol. 65, no. 8, pp. 2698–2710, Aug. 2017.

[34] D. Jiao and J. M. Jin, *Finite Element Analysis in Time Domain, in The Finite Element Method in Electromagnetics*. Hoboken, NJ, USA: Wiley, 2002, ch. 12.

[35] L. Xue and D. Jiao, "Method for analytically finding the nullspace of stiffness matrix for both zeroth-order and higher order curl-conforming vector bases in unstructured meshes," *IEEE Trans. Microw. Theory Techn.*, vol. 68, no. 2, pp. 456–468, Feb. 2020.

[36] A. Brandt, S. McCormick, and J. Ruge, *Algebraic Multigrid (AMG) for Sparse Matrix Equations, in Sparsity and its Applications*. Cambridge, U.K.: Cambridge Univ. Press, 1983.

Li Xue received the B.S. degree in information engineering from Zhejiang University, Hangzhou, China, in 2015, and the Ph.D. degree in electrical and computer engineering from the On-Chip Electromagnetics Group, Purdue University, West Lafayette, IN, USA, in December 2020.

She has been a Research and Development Engineer with the Prime Shield Team, Synopsys, Sunnyvale, CA, USA, since 2020. Her research interests include computational electromagnetics, fast and high-performance algorithms, and high-capacity numerical methods.

Dr. Xue was a recipient of the Best Student Finalist Award from the IEEE International Microwave Symposium in 2019, the Best Student Finalist Award from the Antennas and Propagation (APSURSI) IEEE International Symposium, and the Bilsland Dissertation Fellowship in 2020.

Dan Jiao (Fellow, IEEE) received the Ph.D. degree in electrical engineering from the University of Illinois at Urbana–Champaign, Champaign, IL, USA, in 2001.

She then worked at the Technology Computer-Aided Design (CAD) Division, Intel Corporation, Santa Clara, CA, USA, until September 2005, as a Senior CAD Engineer, a Staff Engineer, and a Senior Staff Engineer. In September 2005, she joined Purdue University, West Lafayette, IN, USA, as an Assistant Professor with the School of Electrical and Computer Engineering, where she is currently a Professor. She has authored three book chapters and over 320 papers in refereed journals and international conferences. Her current research interests include computational electromagnetics, high-frequency digital, analog, mixed-signal, and radio frequency (RF) integrated circuit (IC) design and analysis, high-performance VLSI CAD, modeling of microscale and nanoscale circuits, applied electromagnetics, fast and high-capacity numerical methods, fast time-domain analysis, scattering and antenna analysis, RF, microwave, and millimeter-wave circuits, wireless communication, and bio-electromagnetics.

Dr. Jiao has served as the reviewer for many IEEE journals and conferences. She was a recipient of the Intel's 2019 Outstanding Researcher Award. She received the 2013 S. A. Schelkunoff Prize Paper Award from the IEEE Antennas and Propagation Society, which recognizes the best paper published in the IEEE TRANSACTIONS ON ANTENNAS AND PROPAGATION during the previous year. She was among the 21 women faculty selected across the country as the 2014–2015 Fellow of Executive Leadership in Academic Technology and Engineering (ELATE) at Drexel, a national leadership program for women in the academic STEM fields. She has been named a University Faculty Scholar by Purdue University since 2013. She was among the 85 engineers selected throughout the nation for the National Academy of Engineering's 2011 U.S. Frontiers of Engineering Symposium. She was the recipient of the 2010 Ruth and Joel Spira Outstanding Teaching Award, the 2008 National Science Foundation (NSF) CAREER Award, the 2006 Jack and Cathie Kozik Faculty Startup Award (which recognizes an outstanding new Faculty Member of the School of Electrical and Computer Engineering, Purdue University), a 2006 Office of Naval Research (ONR) Award under the Young Investigator Program, the 2004 Best Paper Award presented at the Intel Corporation's Annual Corporate-Wide Technology Conference (Design and Test Technology Conference) for her work on generic broadband model of high-speed circuits, the 2003 Intel Corporation's Logic Technology Development (LTD) Divisional Achievement Award, the Intel Corporation's Technology CAD Divisional Achievement Award, the 2002 Intel Corporation's Components Research the Intel Hero Award (Intel-wide she was the tenth recipient), the Intel Corporation's LTD Team Quality Award, and the 2000 Raj Mittra Outstanding Research Award presented by the University of Illinois at Urbana–Champaign. She served as the General Chair for the 2019 IEEE MTT-S International Conference on Numerical Electromagnetic and Multiphysics Modeling and Optimization (NEMO), Boston, MA, USA. She was selected as an IEEE MTT-Society Distinguished Microwave Lecturer in 2020. She is an Associate Editor of the IEEE TRANSACTIONS ON COMPONENTS, PACKAGING, AND MANUFACTURING TECHNOLOGY and the IEEE JOURNAL ON MULTISCALE AND MULTIPHYSICS COMPUTATIONAL TECHNIQUES.